A bioinspired soft manipulator for minimally invasive surgery

T. Ranzani[*], G. Gerboni, M. Cianchetti and A. Menciassi

The BioRobotics Institute, Scuola Superiore Sant'Anna (SSSA), Viale Rinaldo Piaggio 34, 56025 Pontedera (PI), Italy
[*]*Corresponding author:* t.ranzani@sssup.it

Abstract

This paper introduces a novel, bioinspired manipulator for Minimally Invasive Surgery (MIS). The manipulator is entirely composed of soft materials and it has been designed to provide similar motion capabilities as the octopus's arm, in order to reach the surgical target while exploiting its whole length to actively interact with the biological structures. The manipulator is composed of two identical modules; each of them can be controlled independently and it is provided with multi-directional bending and stiffening capabilities, like an octopus tentacle. In previous works from the authors the design of the single module has been addressed. Here a 2-module manipulator is presented, with the final aim of demonstrating the enhanced capabilities that such a structure can have in comparison with rigid surgical tools currently employed in MIS. The performances in terms of workspace, stiffening capabilities and generated forces are characterized through experimental tests. The combination of stiffening capabilities and manipulation tasks is also addressed to confirm the manipulator potential employment in a real surgical scenario.

1 Introduction

In the last years the robotic community demonstrated increasing interest in Nature and natural principles as a source of inspiration for developing disruptive innovation in variegated sectors. Looking at Nature achievements it is reasonable in order to try to understand and replicate animal capabilities by deriving and "stealing" the basic concepts which enable such behaviors. Natural manipulators, such as elephant trunks, octopus arms, squid tentacles and snakes have been widely considered as a model for the development of innovative robotic devices or for the improvement of performance of traditional devices (e.g. in terms of locomotion or grasping) [1][2]. In particular, the study of how animals use soft body parts to move in complex, unpredictable environments can provide useful design tools for robotic applications in particularly challenging scenarios, such as medicine, search and rescue, disaster response, and human assistance [3].

The main advantage of such natural systems is the compliance in the interaction that provides adaptability to unstructured environments which can be hardly obtained with conventional stiff structures [3]. In addition, these biological systems can manipulate objects while controlling the stiffness of selected body parts and thus being inherently compliant with the full length of their arm/body. For this reason they have inspired the development of novel soft robotic arms and manipulators [2], [3]. In literature several attempts are presented and they can be grouped into three main categories: discrete hyper-redundant, hard continuum, and soft [2]. For general purpose devices the first two categories are generally preferred such as in the case of the OCRobotics Snake-Arm [4], the OCTARM [5] and the FESTO Bionic Handling Assistant [6]. On the other hand, when for specific applications a down-scaling is needed, these kinds of systems start suffering from disadvantageous scale laws. Moreover applications which imply a high degree of human interaction are often prohibitive for such systems. When safety, flexibility and compliance are desirable features, soft robotics appears as the right answer to these requirements. Examples of different approaches which could partially meet these needs are represented by the Harvard pneumatic tentacle-like soft manipulator [7], the MIT jammable manipulator [8] and the unique concept introduced with the OCTOPUS robot arm, a manipulator which completely relies on soft materials but it is still able to elongate, shorten, bend in any direction and tune its stiffness [9]. Such capabilities are enabling safe and controlled interaction with the biological environment, paving the way to a novel approach in manipulator design.

In the medical field, and in particular in surgical applications, soft robotics represents a promising technology [3], [10]. The use of soft technologies in surgery can lead to the development of novel instrumentation able to overcome limitations of current systems [10]. Similarly to biological manipulators, a soft tool could perform a compliant interaction with tissues; in addition, by exploiting a variable stiffness mechanism, it could actively interact with surrounding structures. Soft and shrinkable devices for self-

propulsion in the gastrointestinal tract are reported in [11], [12], but this class of systems have limited surgical and manipulation abilities.

On the other hand, the requirements of minimally invasive surgical (MIS) procedures, combined with the need of accessing different target organs from sites that are not positioned in the optimum locations with respect to the entry access [13], claim for soft manipulators with locomotion abilities, safe interaction and tunable stiffening. In MIS, access to the surgical target can be performed from 3-5 insertions in the inflated abdomen (i.e. laparoscopy), from a single access exploiting the umbilicus to insert all the necessary instruments from the same access, or from natural orifices. For such procedures, rigid or semi-rigid tools may lead to significant clashing thus increasing the complexity of the procedures [14]. For this reason articulated flexible instruments have been proposed in different body districts such as heart [15], throat [16], [17], brain [18] or in the abdomen through single port access [19] or through natural orifices [20]. Recently, the issue of monitoring the contacts of articulated robots with compliant environments has been addressed in [21]. In this work, the authors proposed a new controller for compliant motion of continuum robots without knowledge of contact locations in order to be safer during the navigation within the body structures.

By merging the technologies of diagnostic endoscopes with compliant structure and the peculiar needs of surgery in remote areas, interventional endoscopes have been proposed since they allow reaching the surgical target while being inserted remotely or by a natural orifice [22]. However, endoscopes may suffer from stability issues due to the lack of a stiffness control [23]. In addition, their interaction with the surrounding is mainly driven by the mechanical properties of its body since only the distal part is actively controlled. Endoscopes able to lock their shape have been proposed by USGI Medical, Inc., San Clemente, CA, USA [24] [25], but still they do not envisage a controlled interaction with the tissue during the insertion phase.

Variable stiffness robots for surgery have been proposed in [26] - [28]. Such systems present a softer structure with respect to articulated instruments, but they exploit the variable stiffness variation mainly for freezing the configuration of the robot and for passing through the surgical instruments.

In this paper a surgical manipulator composed of soft materials inspired from the motion and manipulation capabilities of the octopus is presented. The idea is to develop an instrument able to perform elongation, multidirectional bending and squeezing of its structure in order to be able to reach remote body districts and there manipulate organs. In addition, similarly to what the octopus really does, selective stiffening of its segments can be exploited to modulate the interaction of the manipulator at different levels of the arm. This could lead to the possibility to exploit the length of the manipulator to perform multiple tasks with the same arm. For example, a part of the arm can be exploited for keeping an organ shifted and the other one to operate behind it. Such feature could decrease the number of instruments necessary for performing the surgical intervention.

The presented manipulator is inspired from the motion capabilities of the octopus arm, but in order to meet the requirements in terms of possible actuation technologies, necessary force and motion ranges, different technologies – also not bioinspired - were used as discussed in [10].

In our previous works [10], [29], the overall idea is introduced: the structure of the manipulator is based on a modular architecture where several modules are serially connected and each one presents the capability to be independently actuated and stiffened. In [29] the design of a single module is presented and characterized in all its functionalities. Here, a two module manipulator is presented and characterized. The second module allows verifying the feasibility of the proposed manipulator and in particular to study how stiffness variation can affect its performances.

1.1 The surgical rationale

Traditional surgical tasks imply the use of multiple specialized instruments such as graspers, retractors, vision system, dissectors etc. to carry out a single procedure. All these instruments need to be provided at the surgical site from different access points in the case of laparoscopy, or by using multifunctional instruments in the case of single access procedures. In particular, organ retraction is typically needed for shifting or lifting organs in order to generate the necessary space for passing through other instruments or for exposing the target organ [30], [31]. Retraction tasks can be rethought if the surgical manipulator belongs to this new kind of flexible structures. As an example, Figure 1a illustrates a simplified surgical scenario where, by means of the manipulator's body itself, an organ (depicted in red) can be both lifted up and supported. Therefore by wrapping it and becoming stiffer (yellow line), the manipulator accomplishes the retraction task, which traditionally requires the insertion of additional instruments for moving and securing the organ away from the operative site. Furthermore, the shape of the manipulator would nicely enclose the organ,

without resorting to the employment of clips and graspers which are traditionally used to retract organs during MIS [36], [37].

By means of the same strategy, other tasks such as squeezing into tiny spaces and approaching difficult-to-reach anatomical districts can potentially be accomplished with a single manipulator. Referring to the scheme in Figure 1b, for gaining the necessary space for operating on the green target the manipulator must first slide into the tiny space left above the red organ, then shift and keep the red organ aside, and finally it can manipulate the target. The manipulator's proximal portion has to become stiffer to serve as a stable base for the further manipulation tasks performed by the distal portion.
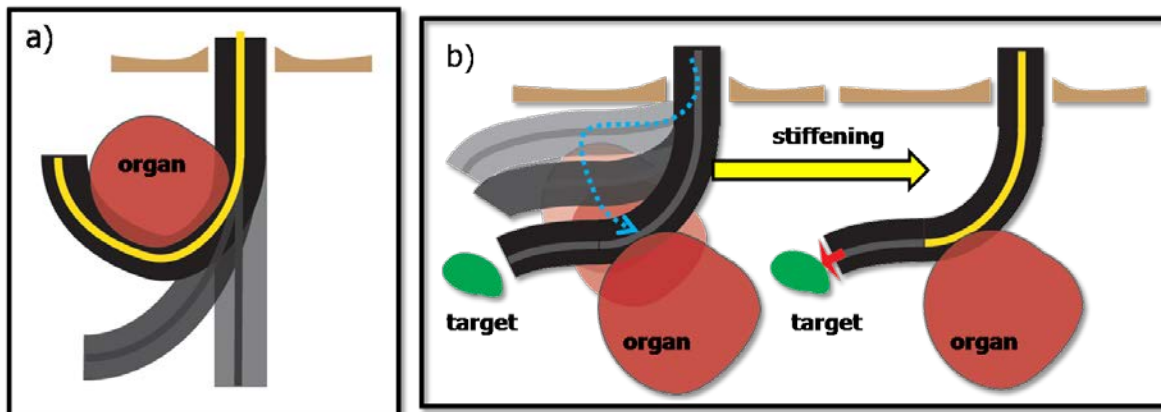
Figure 1: Schematic examples of surgical tasks performed by a tentacle-like structure. a) Organ retraction, showing the manipulator grabbing and lifting up of the organ. b) Fitting in tiny spaces, shifting down of an organ with the base portion and reaching the surgical target with the distal module. The yellow line indicates the stiffening of the manipulator portion.

2 Concept and design of the 2-module manipulator

The soft manipulator is ideally composed of multiple modules each one provided with actuation and stiffening capabilities. A structure composed of an optimized number of modules for a specific surgical application is currently out of the scope of the paper. In this paper, starting from the design of the single module [29] we extend to a 2-module manipulator. This step is particularly significant since it allows – with a minimum number of modules - for testing the combined performances of two interconnected modules in terms of stiffening and actuation.

The manipulator is composed by two connected identical modules. The single module possesses an active motion based on flexible fluidic actuation while stiffening is obtained by exploiting a granular jamming based mechanism.

The design of the actuation system is based on three fluidic chambers equally spaced in radial arrangement embedded in a silicone matrix (Silicone 0050, Ecoflex, Smooth on Inc.) as shown in Figure 2 (right). Multi-directional bending and elongation of the silicone cylinder can be achieved by combining the inflation of the three chambers. Actuating a single chamber leads to the bending in one direction, actuating two chambers at the same pressure will generate a bending in the plane in between the two chambers; finally, the inflation of all the chambers together with the same pressure will cause the elongation of the cylinder along its main axis. Intermediate combinations of the pressure in the three chambers allow reaching different intermediate module configurations. An external crimped sheath is fit around the actuator to contain the lateral expansion of the fluidic chambers during inflation as detailed in [29]. The concept of using fluidic actuators in parallel configuration to obtain multi-directional bending and elongation has been explored in literature: for example the Festo Bionic Handling Assistant utilizes a similar strategy to control the position of their manipulator as well as the force exerted on the environment [6] [potreste metterci qualche altra ref?].

A granular jamming based stiffening mechanism was exploited for stiffness control. Such strategy has already been validated in several robotic devices [8], [32] - [34]. Particularly relevant is the manipulator

described in [8] that also uses coffee as the granular material and allows for the stiffness control of individual modules using vacuum control.

In the proposed manipulator the granular jamming based stiffening system is used in combination with flexible fluidic actuation; this approach has been validated also for different applications in [33], [35]. In Figure 2 an overview of the single module together with its relevant dimensions is reported.

In this paper the 2-module manipulator is presented and characterized. In order to preserve the modularity of the structure, pipes for air supply and vacuum to the second module were left external to the structure.
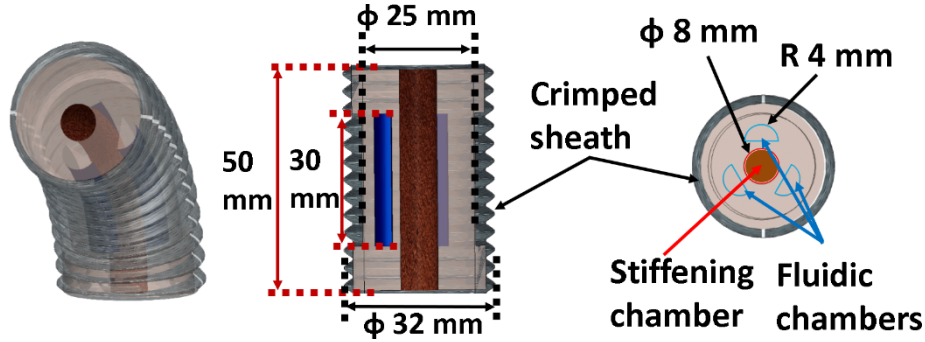
Figure 2: Structure and relevant dimensions of the single module [29]. (Centre) section of the manipulator, the central channel for the granular jamming stiffening mechanism is highlighted. On the right the top view of the module is reported together with its relevant dimensions.

3 Fabrication of the manipulator

3.1 Fabrication of the modules

The body of the module is fabricated via moulding of Silicone (Silicone 0050, Ecoflex, Smooth on Inc, Shore Hardness = 00-50, 100% linearized Tensile Modulus = 83 kPa). A crimped sheath is put around the module in order to contain the ballooning effect due to the chambers inflation. Details on the fabrication process of the single module can be found in [29].

Each module integrates in the central channel a granular jamming based stiffening mechanism composed of an external latex membrane filled with 6 g of coffee; a 2 mm pipe is inserted inside and the membrane is sealed around it with Parafilm. The stiffening chamber is extended of approximately 5 mm on both sides with respect to the module length as shown in Figure 3. This feature allows for keeping the stiffness variation capability even in the junction between the two modules by guaranteeing that the granular material will be present also in this portion. Each stiffening chamber has a cylindrical shape once integrated in the module, thus considering a volume of $L * \pi * r^2$ (where L is the length on the module, 50 mm plus the extra lengths and r is the radius of the stiffening chamber) the resulting density at rest condition is 1.8×10^3 Kg/m^3. The coffee used is coarse coffee in line with [8].

The pipes used both for inflating the fluidic chambers and for vacuuming the stiffening chamber are 2 mm in outer diameter and 1.2 mm in inner diameter polyurethane tubes (SMC Corporation). They are connected to the fluidic chambers after the fabrication of the modules. In order to avoid possible leakages, Sil-Poxy silicone rubber adhesive (Smooth on Inc.) is used to glue them in the silicone channel used for supplying air to the fluidic chambers. In order to increase the adhesion of the pipes, their tip is scratched with sandpaper.

The total length of the manipulator is given by the length of the two modules (50 mm), plus 10 mm of junction, 10 mm of the tip and 15 mm on the base.

A bioinspired soft manipulator for minimally invasive surgery
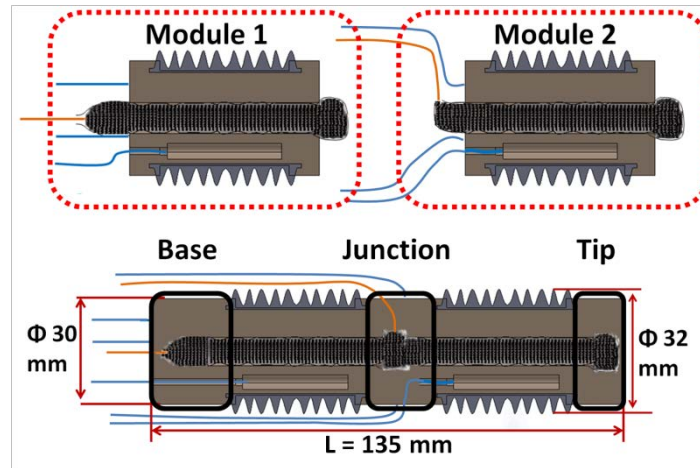
Figure 3: Fabrication steps of the multi-module manipulator. Top, section of the two modules before connection. Bottom: two interconnected modules. In blue the pipes for the fluidic actuation; in orange the pipes for supplying vacuum to the stiffening chambers.

3.1 Modules connection and junction design

The inter-module connection is performed by putting the modules, with the fluidic chambers aligned, at 1 cm distance. This will imply that the part of the stiffening chamber coming out from top and bottom of the modules will be in contact and slightly compressed among each other. Two half cylindrical shells with an inner diameter of 32 mm are then closed on the junction and Silicone (Silicone 30, Dragonskin, Smooth on Inc, Hardness = 30, 100% linearized Tensile Modulus = 593 kPa) is poured inside. The same procedure is repeated on the top and bottom parts of the manipulator, in order to fully close the structure (Figure 3 bottom). The base is extended of 1.5 cm in order to simplify the clamping of the manipulator during the testing phase.

The use of a stiffer silicone material in the passive parts and particularly in the junction area, guarantees that they don't affect the overall behaviour of the manipulator.

Dragonskin 30 silicone was chosen since it presents a stiffness approximately 7 times higher than Ecoflex 0050 which is used for the fabrication of the modules. The mechanical properties of the two silicones were tested according to ISO 37:2005(E) and the stress - strain data are shown in Figure 4. The curves of Figure 4 represents the average of five cycles of loading/unloading of the silicone performed with an Instron 5900 Testing System at 0.1 mm/min speed and imposing 200% strain. The maximum measured variability was ± 3.4 kPa for the Ecoflex 0050 and 2.8 kPa for the Dragonskin 30.
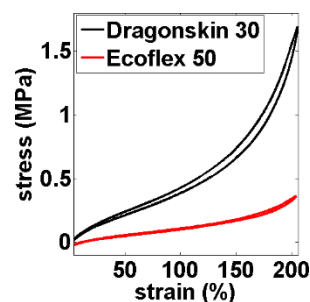
Figure 4: Stress-strain test results of Silicone Ecoflex 0050 and Silicone Dragonskin 30.

4 Materials and methods

The characterizations performed on the manipulator are hereby presented. The manipulator is characterized through experimental characterizations aimed at verifying its dexterity, stiffening capability and possibility of exploiting stiffness variation during the application of forces. Kinematic and dynamic modelling are out of the scope of the present paper.

A bioinspired soft manipulator for minimally invasive surgery

4.2 Experimental characterization

The actuation of the 2-module manipulator was performed by controlling the pressure in each fluidic chamber independently. Six proportional pressure regulator valves (series K8P, E.V.P. systems) were used to modulate the air pressure inflated in each chamber from 0.0 to 0.065 MPa (inset of Figure 5). A compressor (Compact 106, Fiac Air-Compressors) was used as pneumatic air source. Vacuum for stiffness modulation was obtained by vacuum regulators (ITV0090, SMC Corporation), shown in the inset of Figure 5, and a vacuum pump (LB.4, D.V.P. Vacuum Technology). The vacuum pump is able to provide a maximum vacuum of 0.03 Pa absolute pressure with a flow of 3 m^3/h. The vacuum generated inside the stiffening chamber was monitored with a pressure sensor (SWCN-V01-P3-2, Camozzi) and resulted in a maximum of −0.0987 MPa relative pressure. A 5 µm filter (MC104-D10, E.V.P. systems) was used to prevent particles to enter into the pump.

The control of the pressure and vacuum regulators is done with lowpass filtered PWM signals generated from the digital I/O pins of the RoNex MkII (http://www.shadowrobot.com/products/ronex/). The pressure within each chamber can be regulated by setting the period and the ON-time of the PWM signal for each pin. The RoNex MkII is programmed using Robot Operating System (ROS). The components for the control of the manipulator are illustrated in Figure 5. During the tests, the manipulator was fixed with the clamping system shown in Figure 5.
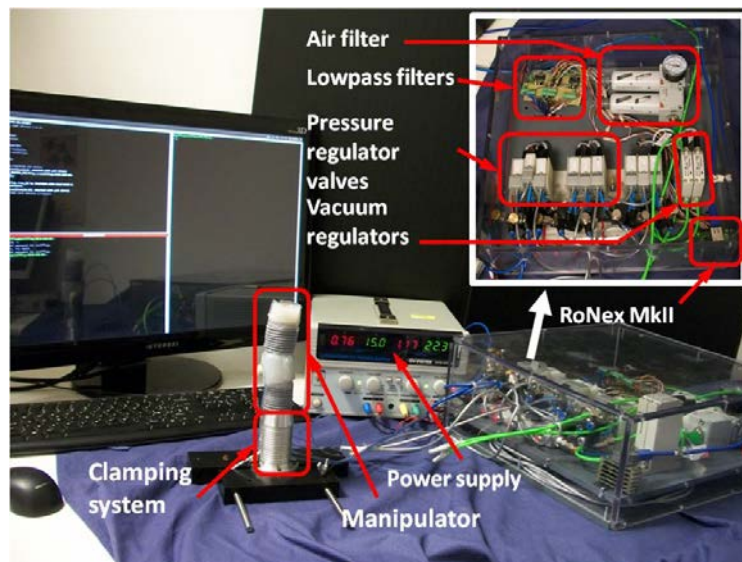
Figure 5: Setup for the active motion and stiffening of the 2-module manipulator. In the inset the top view of the box is shown, indicating all components used for the control of the pneumatic actuation and of the vacuum levels.

4.2.1 Workspace evaluation

The workspace of the 2-module manipulator was obtained from the extension of the single module one. The workspace of the single module was obtained by placing a 6-DOF probe (Northern Digital Inc.) on the tip of a single module and measuring the position and orientation of the tip at all the different pressure combinations in the three fluidic chambers (Figure 6, left). The pressure range tested in the chambers was from 0.0 to 0.065 MPa. Since the module motion in response to the applied pressure is not linear, the following pressures were tested, [0.00 0.025 0.035 0.045 0.050 0.065] MPa. These pressures were experimentally found to significantly describe the motion of the module in previous works. All the different combinations of the aforementioned pressures were applied in the three chambers, thus realizing 63 combinations (i.e. 216 points). Each pressure combination was automatically set by the control system in ROS; between two pressure combinations the pressure was reset to 0.0 MPa in all the chambers. During the application of each combination of pressures, the position and orientation of the module tip was acquired with the Aurora® EM Tracking system for 1 s (i.e. 100 samples).
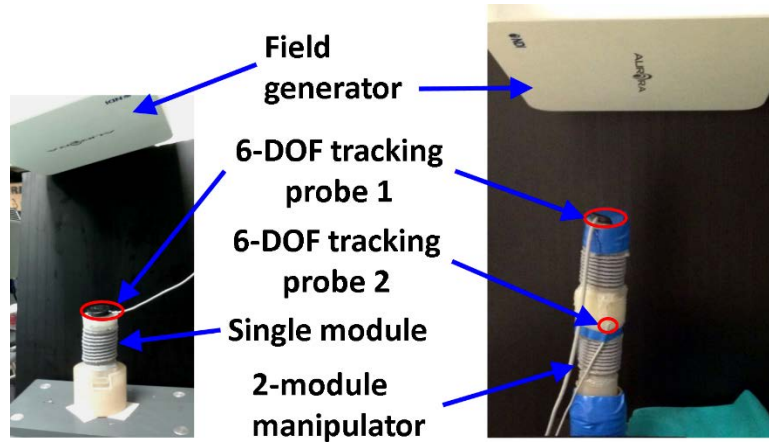
Figure 6: Left, setup for the experimental measurement of the workspace of the single module. Right, setup used for the experimental measurement of specific configurations of the 2-module manipulator. The 6 DoF localization probe (Northern Digital Inc.) is highlighted in red in the picture.

The workspace of the two module manipulator was computed from such data by considering for each point reached from the first module, all the possible configurations of the second one.

In Figure 7, the procedure is shown in an exemplified scenario; the coordinate system o is the world coordinate system. The localization probe measures the position and orientation of the coordinate system o' for each point of the workspace of the single module (with the Aurora tracking system). The transformation matrices from the coordinate system o to o' are computed from these experimental data. Assuming that the two modules composing the manipulator are identical, the two transformation matrices T_{01} (from world coordinates to first module tip) and T_{12} (from first module tip to second module tip) can be considered identical. The orientation and position of o'' (for every configuration) can be obtained by multiplying each T_{01} (one for every point of the first module workspace) for all the T_{01}. The junction area is considered as an extra translation matrix in the local coordinate system o'.

In Figure 7, some explicative configurations of the system are drawn. In configuration 1 (no actuation, rest condition), the position of the tip of the second module is obtained by a simple translation along the z_1' axis. When the first module is bent (configuration 2), applying the same transformation as before the point o_2'' can be obtained. Similarly, when even the second module would be bent the same transformation that maps o into o_2' can be used on o_2' to obtain o_3''.
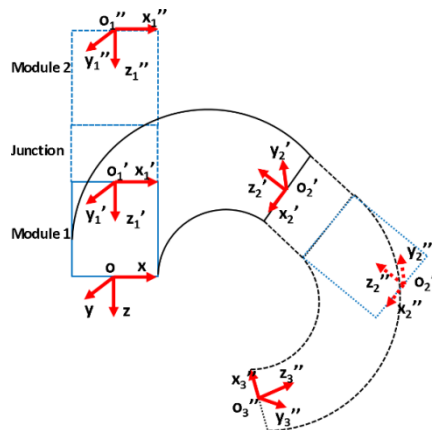
Figure 7: Scheme of the extrapolation strategy for computing the workspace of the 2-module manipulator form the workspace of the single module. The world coordinate system is o, the local coordinate system of the first module is o' and the local coordinate system of the second module is o''.

Some relevant configurations of the manipulator, including elongation, bending with single chamber actuation and bending with two chambers actuation, were measured experimentally in order to characterize the effective behaviour of the manipulator and compare them with the data obtained by extending the workspace of the single module. Such measurements were performed by placing two 6-DOF probes on the manipulator, one at the tip and one at the end of the first module as shown in Figure 6, right. In all cases the inflation pressures tested were [0.00 0.025 0.035 0.045 0.050 0.065] MPa. In the case of single chamber bending one chamber of each module was inflated at the same time (Figure 8a), for the two chamber bending two chamber per module were pressurized by the same value and at the same time (Figure 8b) while for the elongation measurement all three chambers of the two modules were inflated by the same pressure at the same time (Figure 8c)
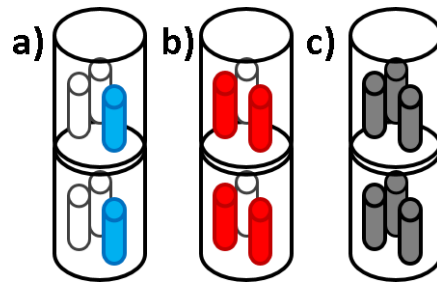
Figure 8: Scheme of the 2-module manipulator highlighting the chambers activated for single chamber bending (a), two chambers bending (b) and elongation (c)

4.2.2 Junction characterization

The mechanical properties of the junction area between the two modules were experimentally characterized using the setup shown in Figure 9. The active parts of the 2-module manipulator were fully constrained with two rigid shells and a fixed displacement was imposed to the tip of the manipulator by a 6 DOF industrial robot (RV-6SL, Mitsubishi) with an F/T sensor (MINI 45, ATI, USA, resolution = 0.025 N) fixed on its end effector. In this way the overall deflection was due only to the behaviour of the junction area as schemed in Figure 9, right. The test was performed at different vacuum pressures in the stiffening chamber, i.e. 0.0 MPa, −0.052 MPa and −0.098 MPa in both the stiffening chambers of the two modules; each test was repeated three times.
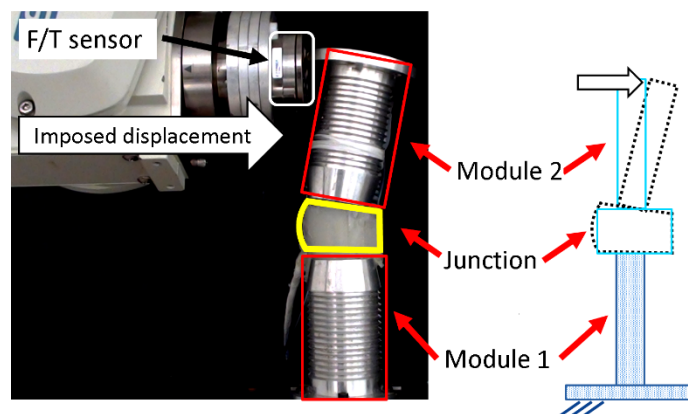
Figure 9: Setup for the experimental characterization of the junction are between the two modules. Left, assembled setup; in red the modules composing the manipulator are indicated, in yellow the deformed junction is highlighted. Right, scheme of the system.

4.2.3 Stiffness Characterization

The stiffening capabilities of the single module in different configurations in terms of bending and elongation have been extensively characterized in [29]. In this paper the stiffening capabilities of the

manipulator as a whole are presented. Tests were performed imposing different displacements at the tip of the manipulator by using a 6 DOF industrial robot (RV-6SL, Mitsubishi) with an F/T sensor (MINI 45, ATI, USA, resolution = 0.025 N) fixed upon its end effector. In that way it has been possible to impose the right orientation of the load cell respect to the module tip position. The same test was performed when the stiffening mechanism was not activated (0.0 MPa) and when -0.098 MPa vacuum was induced in the granular jamming based stiffening mechanism; each test was repeated 5 times on two manipulators. The stiffness variation was characterized both in compression and tensile tests. Compression tests were performed compressing the manipulator along the z direction, Figure 10a, of 5 mm. The same compression test was performed when the first module is 90° bent by inflating one of its chambers with a pressure of 0.045 MPa (Figure 10b). Tensile tests were performed imposing a lateral displacement to the manipulator. Such tests were carried out at different bending angles (Figure 10c). The tests at different bending angles were performed inflating one chamber on each module with the same pressure (Figure 8a); the tested pressures were [0.00 0.025 0.035 0.045 0.055 0.065] MPa.
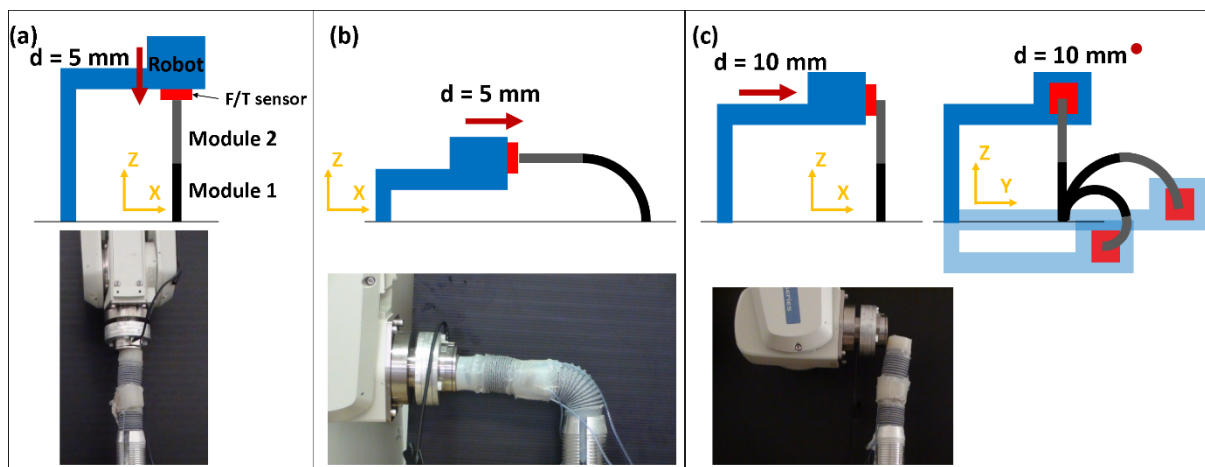
Figure 10: Manipulator configuration tested for evaluating the stiffening capabilities. The red square represents the F/T sensor, the blue one represents the robot end effector; the base module of the manipulator is the black one and the second module is the dark grey one. a) Axial test, b) axial test with the first module 90° bent, c) lateral test at different bending angles of the manipulator (left, side view; right, front view). For each configuration the photo of the real setup is reported below.

4.2.4 Combined force and stiffening experiments

Two different typologies of tests were carried out to evaluate the forces exerted by the manipulator exploiting the selective stiffening capabilities of its segments. The first test consisted in positioning the manipulator in the same configuration as for the stiffening tests, Figure 10c, with the tip in contact with the F/T sensor mounted on the robot arm. Three different vacuum levels ([0 −0.052 −0.098] MPa) were imposed in the first module (shown in black in Figure 10c); for each vacuum level, the chamber of the second module (shown in grey in Figure 10c) that causes a bending on the x-z plane, was inflated at [0.025 0.035 0.045 0.055 0.065] MPa to press against the F/T sensor. Forces were measured using an F/T sensor (NANO17, ATI, USA, resolution = 0.00625 N). The same procedure was performed while stiffening the second module and actuating the first one.

The second typology of tests aims at exploiting the stiffening capabilities together with the possibility to generate forces in a more surgery-like scenario. Although the previous described test provided a good overview of the two modules manipulator, they still lack in thoroughly demonstrate the real capabilities of such a structure, in comparison with traditional rigid link surgical manipulators.

For that reason, scenarios as proposed in the schematic view of Figure 1 have been taken as guidelines to build a more reliable, credible testing set up for the 2-module manipulator. To reproduce the compliance, in terms of weight and shape of organs or anatomical parts, that the manipulator may encounter during a

surgical laparoscopic procedures, water filled balloons have been employed and they have been placed around the manipulator to test its interaction with them.

Among the variety of possible tasks, a few key movements were chosen to demonstrate the manipulation and stiffening capabilities. These are the wrapping and retraction of a water filled balloon (800 g, Figure 18a), hung up to a load cell which revealed when the whole weight of the balloon was supported by the manipulator. Another task is shown in Figure 18b where the manipulator navigates among compliant objects (water filled balloons), embraces one of them (270 g) and moves it aside. The last task, presented in Figure 18c demonstrated the manipulator supporting a weight of 500 g with the first module and applying a force on an F/T sensor. The same test is performed without stiffening activation and when the first module is fully stiffened. In this last experiment two F/T sensors were used. One F/T sensor is connected to the water filled balloon (5 N), while the other is positioned in the proximity of the distal end of the manipulator. In this test, two pieces of information can be extracted. The first F/T sensor allows verifying that the water filled balloon is completely supported, while the second F/T sensor measures the amount of force generated on the target.

5 Results and discussions

In this section the results obtained from the characterizations described in Section 4 are presented. Figure 11 shows the fabricated 2-module manipulator.
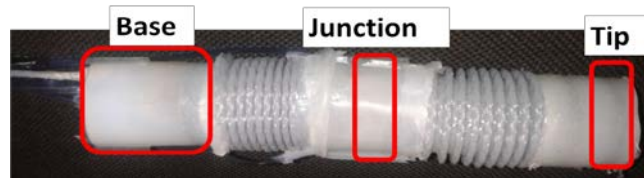
Figure 11: Fabricated 2-module manipulator.

5. 1 Workspace evaluation

In Figure 12 the full workspace of the 2-module manipulator is shown. In Figure 12a, a section of the workspace is reported; the section cuts in two parts the workspace on the *x*-plane in order to have a clearer visualization. The initial position of the manipulator (no actuation) is schemed in the plot as a cylinder. The arc drawn by the points on the left side of Figure 12a corresponds to the single chamber bending and in agreement to the results obtained with the single module in [29] higher curvatures can be achieved and lower points in the *z* direction can be reached (-75 mm with respect to the base of the manipulator). The right side of Figure 12a correspond to the two chambers bending and presents a bigger radius of curvature. The experimental trajectories of the tip of the 2-module manipulator during single chamber bending (cyan), two chambers bending (red) and elongation (black) are overlapped to the extrapolated data. In Figure 12b the unreachable areas inside the workspace are highlighted; the yellow area is below the single chamber bending and thus it extends slightly less than the red area which is in correspondence to the two chambers bending. In Figure 12c the top view of the full workspace is reported. The planes corresponding to single and double chamber bending are highlighted in cyan and red respectively. The system presented good symmetry properties (with 120° phase) in its behavior.

The maximum diameter of a circle containing the whole workspace in the *x-y* plane (Figure 12c) is 312.4 mm.

A bioinspired soft manipulator for minimally invasive surgery
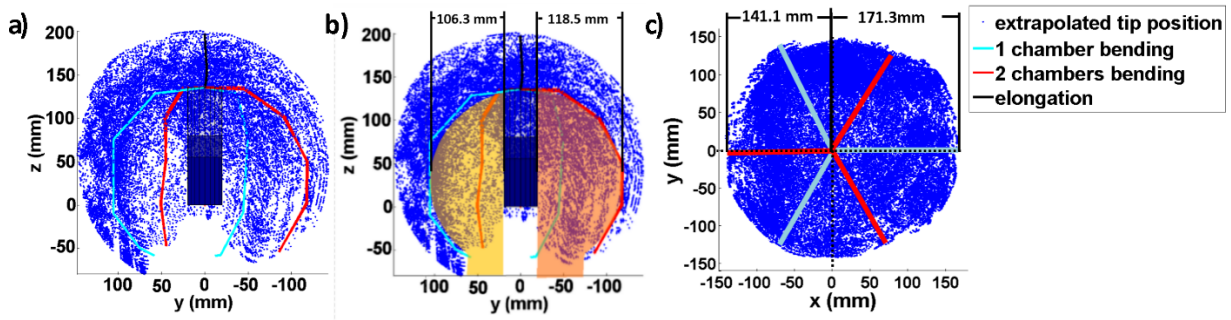
Figure 12: Workspace of the two module manipulator. a) Section of the workspace along the *x* plane, lateral view. b) Section of the workspace with highlighted the unreachable areas. c) Top view of the workspace.

The experimentally measured elongation capabilities of the 2-module manipulator were up to 62%, and match the extrapolated data as evident from Figure 12a. In Figure 13 a photo of the manipulator reaching its maximum elongation is shown.

Figure 13: Left, 2-module manipulator not actuated. Right, fully elongated manipulator with 0.065 MPa the three chambers of each module.

In Figure 14 the results from the single and two chambers bending are reported. Figure 14 a), b) represent the tip trajectories (position and orientation) of the manipulator during single chamber bending and two chamber bending respectively, together with a photo of the manipulator at the correspondent maximum reachable angle. In the plots of Figure 14 a), b) the manipulator is schemed in the non-actuated configuration as a cylinder and the trajectories, derived from the workspace extrapolation, are reported in blue, while the experimental data are in red. The two trajectories follow quite well for small pressures (around 0.04 MPa) after that the error increases considerably, in particular for the *z* coordinate and especially for the two chamber bending trajectory. A very similar trend is followed by the orientations (although the errors are smaller): the estimated bending angle is 236°±3.4° while the measured one is 255°±3.6°. In the case of the two chambers bending, the computed bending angle is 175°±1.8° and the experimentally measured one is 207°±2.3°.

The possible reason for this difference can be found in Figure 14 c), d) where the trajectories of the single (Figure 14c) and two chamber (Figure 14d) bending, measured on a single manipulator (blue) and measured at the end of the first module of the 2-module manipulator (red), are reported. It is evident that the module is more pushed down by the weight of the second module and this effect is intuitively higher at larger bending angles. In addition, the maximum bending angle with single chamber bending of the single module, is 118°±3.2° while in the 2-module manipulator is 132°±2.9°. Similarly the maximum bending angle with two chambers bending of the single module is 87.5°±1.8° while in the 2-module manipulator is 115°±2.2°.

The experimental data suggests that the estimated workspace will present more points at the bottom in reality, but still the estimated workspace is a good first estimate of the manipulator reachable space.
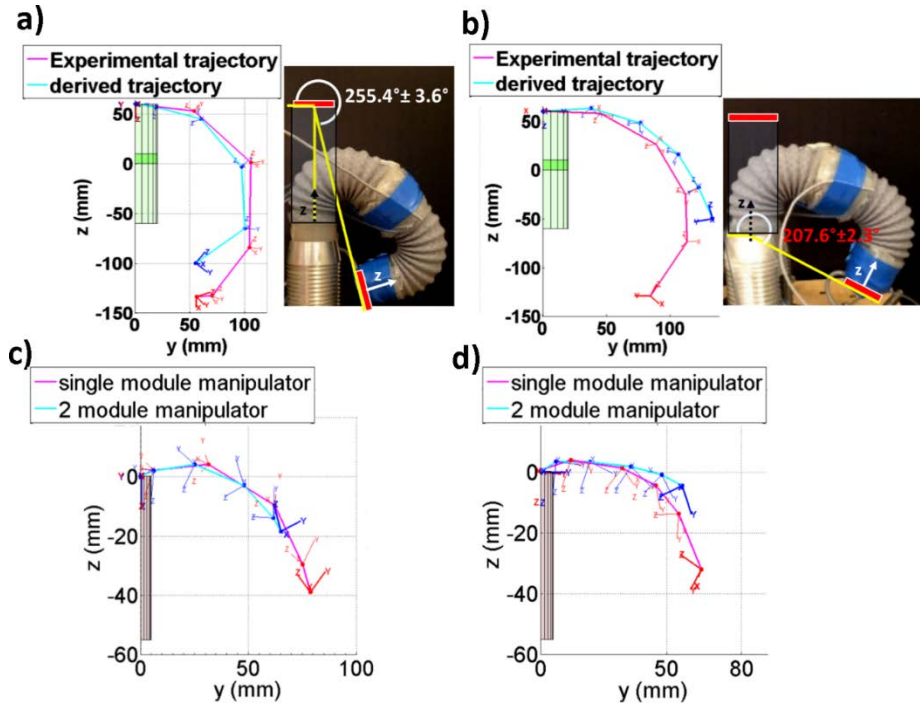
Figure 14: Comparison between experimentally measured trajectories end extrapolated ones. a) Trajectories of the single chamber bending in the 2-module manipulator and photo of the manipulator reaching the maximum bending angle with the single chamber inflation in both modules of 0.065 MPa. b) Trajectories of the two chambers bending in the 2-module manipulator and photo of the manipulator reaching the maximum bending angle with the two chamber inflation in both modules of 0.065 MPa. c) Trajectory during single chamber bending of a single module per se and when integrated in the two module manipulator. d) Trajectory during two chambers bending of a single module per se and when integrated in the two module manipulator

5.2 Junction characterization

In Figure 15 the results for the tests on the junction are reported. The forces necessary to deform the junction area reaches a maximum of 3.07±0.56 N at 10 mm displacement when the stiffening chamber is not activated (0.0 MPa in the stiffening chamber). In the same conditions but applying −0.052 MPa pressure in the stiffening chambers the force increases 5.61±0.08 N (83% increase) and reaches 6.86±0.12 N (123% increase) at −0.098 MPa. The slope of the curves (elastic constants) varies from 0.31 N/mm at atmospheric pressure to 0.54 N/mm at −0.052 MPa and 0.69 N/mm at −0.098 MPa.
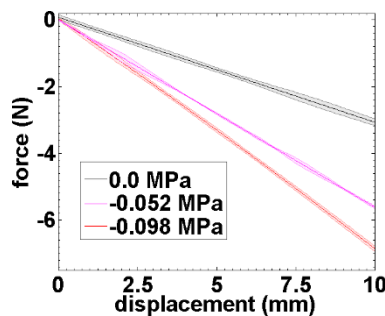
Figure 15: Results from the characterization of the junction between the two modules of the manipulator.

Considering that the average weight of each module was measured to be 28.6±0.7g (corresponding approximately to a force of 0.03 N) it would cause a negligible deformation of the junction according to Figure 15.

A bioinspired soft manipulator for minimally invasive surgery

5.3 Stiffness Characterization

The results from the stiffness tests of Figure 10 are presented in Figure 16. The plots report the force measured from the F/T sensor with respect to the imposed displacement of the manipulator. Three different vacuum levels were applied to the stiffening chamber in order to verify the possibility to tune the stiffness level. As an indication of the stiffness, the elastic constant was computed as the slope of the linear tract of the curves (dashed lines in the plots of Figure 16).

In Figure 16a the results correspond to the configuration of Figure 10a). In this case for the first 2.5 mm displacement the effect of the stiffness variation is not evident. This is probably due to the change in volume of the stiffening chamber that tends to pack the granules together, thus leaving the tip with less granules and with a stiffness similar to the silicone one. On the other hand, it is possible to appreciate the stiffness variation when the displacement increases over 3 mm. In this case the elastic constant was computed as the slope of the curves in the last part of the plot. The elastic constant varies from 2.18 N/mm when no stiffening is activated up to 3.15 N/mm at -0.052 MPa vacuum pressure and 5. 1 N/mm at -0.098 MPa. The average error in the data was 1.3%.

In Figure 16b the results from the axial test when the first module is bent of 90° are reported. In this case the elastic constant varies from 1.99 N/mm when no stiffening is activated, to 2.6 N/mm at -0.052 MPa vacuum pressure and 2. 96 N/mm at -0.098 MPa. It is interesting to observe that the manipulator is able to withstand relatively high forces, also in the bent configuration; in particular it withstood up to 14.6 N at −0.098 MPa vacuum pressure that is relevant for surgical tasks. The average error in the data was 6.2%.

In Figure 16c the results from the lateral tests are reported. The force necessary to deflect the manipulator changes according to the stiffening level. The elastic constant varies from 0.11 N/mm when no stiffening is activated to 0.20 N/mm at -0.052 MPa vacuum pressure and up to 0.31 N/mm at -0.098 MPa.
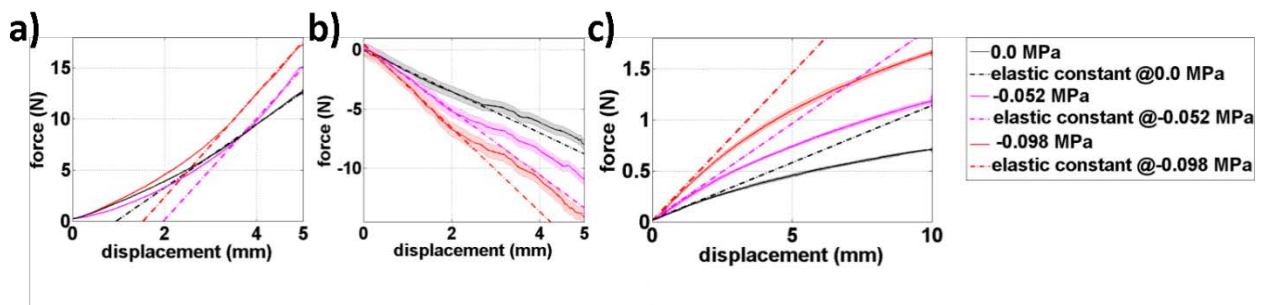
Figure 16: Results from the stiffness tests. a) Axial tests. b) Axial tests with the first module bent 90° (0.045 MPa inflation on one chamber) c) lateral test with no chamber inflation.

The results from all stiffening tests are summarized in Table 1: all the results from the lateral tests (Figure 10c), including the cases when the manipulator is bent with single chamber inflation of both modules (Figure 8a), are reported. The change in the elastic constant in the experiments was computed in the configurations shown in Figure 10. In the last column the percentage of change in the stiffness is reported. It is important to observe that the stiffness variation is maintained also during the bending of the manipulator. As evident from Table 1, the elastic constant decreases due to the bending of the structure; however the stiffening mechanism guarantees (in all the configurations tested) a considerable increase in the stiffness of the manipulator.

Table 1: Summary of the results from the stiffening tests on the 2-module manipulator

Test typology	Chamber inflation pressure in both modules (MPa)	Elastic constant (N/mm) @0.0 MPa pressure (stiffening chamber not active)	Elastic constant (N/mm) @-0.098 MPa pressure (stiffening chamber active)	Elastic constant increase (%)
lateral	0.0	0.11	0.31	66.6
	0.025	0.08	0.14	75

	0.035	0.05	0.15	200
	0.045	0.06	0.17	183.3
	0.055	0.06	0.17	183.3
	0.065	0.07	0.14	100
axial	0.0	2.18	5.10	133.9
	0.045 @module1	1.99	2.96	48.7

5.4 Combined force and stiffening experiments

In Figure 17, the results from the combination of stiffening and actuation are presented. On the left of Figure 17, the case when the second module is actuated to press against the F/T sensor for each vacuum level of the first module (highlighted with dashed lines in Figure 17), is presented. On the right of Figure 17, the case the first module is actuated by inflating a single chamber up to 0.065 MPa for each vacuum level of the second module, is reported.

On the left of Figure 17, the maximum force exerted by the actuated module on the F/T sensor when no stiffening is activated tends to saturate to approximately 1 N. On the other hand, when the base module is stiffened, the force is transmitted more effectively since the higher stiffness of the first module provides a more stable support for the second module (that is applying forces to the F/T sensor). The maximum force when the base module is fully stiffened reaches 2.2 N. This feature is important in order to apply forces in a controlled way to tissues and biological structures. In absence of stiffening capability, if the force necessary to shift a weight is too high, the structure may not succeed and deform in a non-controlled way in other directions due to its highly compliant structure.

On the right of Figure 17, the effect of the stiffness variation is not as effective as in the previous case. This is probably due to the fact that the stiffening system is integrated in the central channel in order to keep the external compliance of the robot, thus its effect is mediated from the soft material in between. However the maximum transmitted force increases from 3.45 N to 4.47 N when the stiffening system is activated.
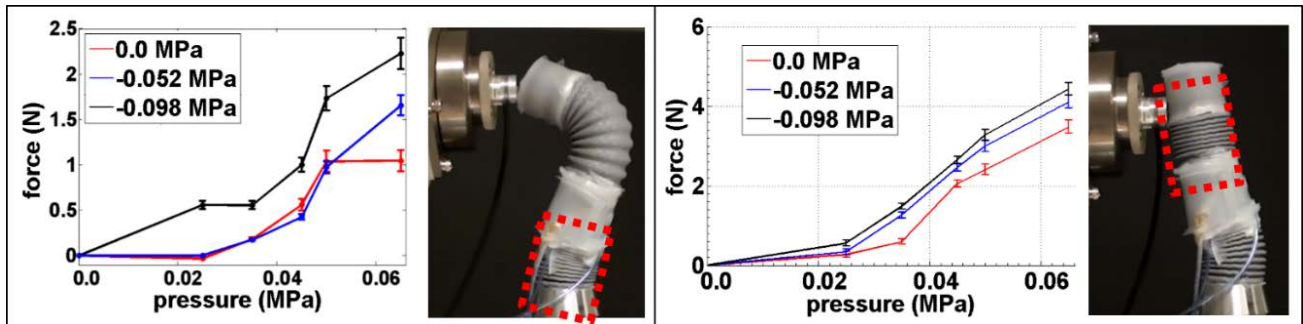
Figure 17: Results from the testing on the combination of actuation and stiffening. (Left) Stiffening of the base module, highlighted with the dashed square, and actuation of the first one. (Right) stiffening of the second module (highlighted with the dashed square) and stiffening of the second one.

In Figure 18 some examples of the 2-module manipulator interacting with water filled balloons are reported. In Figure 18a, the robot is shown while passing below the balloon (500 g) with the first module and exploiting the second module to grasp it and move it around in order to change its position. This could be useful in the surgical scenario to retract an organ and change its position during the surgical operation to make space where necessary. Figure 18b shows the manipulator fitting between two water filled balloons, lifting and shifting one of them to free the access to the other one. Differently from the previous case, the manipulator is inserted from the top. In Figure 18c, the manipulator was able to keep the weight of a 500 g balloon with the first module and apply a force on the F/T sensor. The same test was performed when the first module was not stiffened and when it was stiffened. In the first case the maximum recorded force was 5.83 N, in the second 7.91 N, thus validating the results obtained in Figure 17, left.
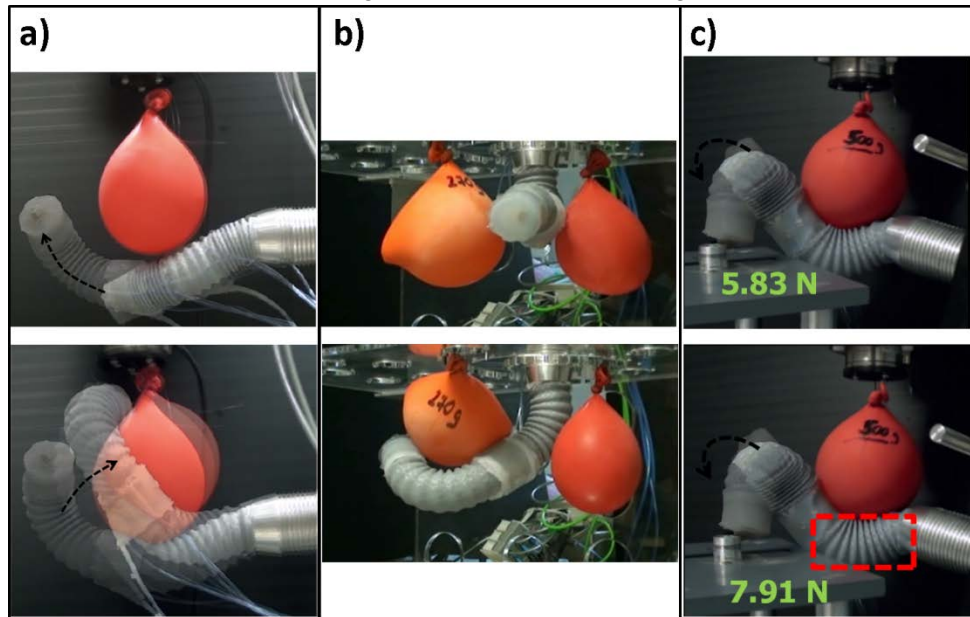
Figure 18: Examples of the 2-module manipulator interacting with water filled balloons and exploiting combined stiffening, dexterity, and force capabilities to perform surgical-like tasks.

6 Conclusion

This paper introduces a 2-module soft, variable stiffness, manipulator for MIS. The manipulator is inspired by the motion capabilities of the octopus and capitalizes in replicating its basic functionalities, which are multi-directional bending, elongation, stiffening and squeezing. We exploited different technologies and materials with respect to the biological counterpart in order to tune it for specific applications as a surgical tool. Flexible fluidic actuation is exploited for the active motion of each module and a granular jamming based stiffening mechanism is used for controlling the stiffness of its segments. Extensive characterization demonstrated that the proposed system is able to provide bending of almost 260° and elongations up to 62%. Selective stiffening of more than 66% was measured, although the shape-locking functionality is not possible yet and it need to be exploited in combination with the actuation system. In addition, some preliminary evaluations on the possibility to tune the stiffness level controlling the vacuum pressure are reported.

The possibility to combine the stiffening of a module and the actuation of the other one was demonstrated to increase the performances of the manipulator, especially in terms of force transmission. Such feature was exploited to perform simulated surgical scenarios where the organs were simulated with water filled balloons. Future works will include an extensive study of the necessary number of modules for effectively performing a specific surgical task and for the optimization of the structure, especially integrating on board valves for avoiding the external pipes for pneumatic supply.

A bioinspired soft manipulator for minimally invasive surgery

Acknowledgments

References

[1] Smith K K and Kier W M 1989 Trunks, tongues, and tentacles: Moving with skeletons of muscle *Am. Sci.* **77** 28–35

[2] Trivedi D, Rahn D C, Kier M W and Walker D I 2008 Soft robotics: Biological inspiration, state of the art, and future research *Appl. Bionics Biomech.* **5(3)** 99–117

[3] Kim S, Laschi C and Trimmer B 2013 Soft robotics: a bioinspired evolution in robotics *Trends in Biotechnol.* **31(5)**287-294

[4] http://www.ocrobotics.com/

[5] Walker I, Dawson D, Flash T, Grasso F, Hanlon R, Hochner B, Kier W, Pagano C, Rahn C, Zhang Q 2005 Continuum robot arms inspired by cephalopods *Proc. SPIE Conf. Unmanned Ground Vehicle Technology* pp 303-314

[6] http://www.festo.com

[7] Martinez V R, Branch L J, Fish R C, Jin L, Shepherd F R, Nunes M D R, Suo Z, Whitesides M G 2013 Robotic Tentacles with Three-Dimensional Mobility Based on Flexible Elastomers *Adv. Mater.* **25(2)** 205-212

[8] Cheng N G, Lobovsky M B, Keating S J, Setapen A M, Gero K I, Hosoi A E, Iagnemma K D 2012 Design and Analysis of a Robust, Low-cost, Highly Articulated manipulator enabled by jamming of granular media *Proc. IEEE Int. Conf. on Robotics and Automation,* pp 4328-33

[9] Laschi C, Cianchetti M, Mazzolai B, Margheri L, Follador M, Dario P 2012 Soft Robot Arm Inspired by the Octopus *Adv. Robotics* **26(7)** 709-727

[10]Cianchetti M, Ranzani T, Gerboni G, Nanayakkara T, Althoefer K, Dasgupta P, Menciassi A 2014 Soft robotics technologies to address shortcomings in today's minimally invasive surgery: the STIFF-FLOP approach. *SoRo* (accepted for publication)

[11]Slatkin A B, Burdick J and Grundfest W 1997 The development of a robotic endoscope *Experimental Robotics IV* **223** 161-69

[12]Phee L, Accoto D, Menciassi A, Stefanini C, Carrozza M C, Dario P 2002 Analysis and development of locomotion devices for the gastrointestinal tract *IEEE Trans. Biomed Eng* **49(6)** 613-16

[13]Vitiello V, Lee S, Cundy T, Yang G 2013 Emerging Robotic Platforms for Minimally Invasive Surgery *IEEE Rev. Biomed. Eng.* **6** 111-26

[14]Vyas L, Aquino D, Kuo C H, Dai J S, Dasgupta P 2011 Flexible Robotics. *BJU Int.* **107** 187-89

[15]Degani A, Choset H, Wolf A, Zenati M A 2006. Highly articulated robotic probe for minimally invasive surgery *Proc. IEEE Int. Conf. Rob Autom.* pp 4167-72

[16]Wei W, Kai X, Simaan N. 2006 A Compact Two-armed Slave Manipulator for Minimally Invasive Surgery of the Throat. *Proc IEEE/RAS-EMBS Int Conf. Biomedical Rob. Biomechatr.* pp 769-74

[17]Bajo A, Dharamsi L M, Netterville J L, Garrett C G, Simaan N 2013 Robotic-assisted micro-surgery of the throat: The trans-nasal approach. *Proc. IEEE Int. Conf. on Robotics and Automation* pp.232-38

[18]Burgner J, Swaney P J, Lathrop R A, Weaver K D, Webster R J 2013 Debulking From Within: A Robotic Steerable Cannula for Intracerebral Hemorrhage Evacuation *IEEE Trans. Biomed. Eng.***60 (9)** 2567-75

[19]Bajo A, Goldman R E, Long W, Fowler D, Simaan N 2012 Integration and preliminary evaluation of an Insertable Robotic Effectors Platform for Single Port Access Surgery *Proc. IEEE Int. Conf. on Robotics and Automation* pp 3381-87

[20]Shang J, Noonan D P, Payne C, Clark J, Sodergren M H, Darzi A, Yang G Z 2011 An articulated universal joint based flexible access robot for minimally invasive surgery *Int. Conf. on Robotics and Automation* pp1147-1152

[21]Goldman R E, Bajo A and Simaan N 2014 Compliant Motion Control for Multisegment Continuum Robots With Actuation Force Sensing. *IEEE Trans. Rob* **99** 1-13

[22]Yeung B P M and Gourlay T 2012. A technical review of flexible endoscopic multitasking platforms. *Int. J. Surg* **10(7)** 345-54

[23]Loeve A, Breedveld P and Dankelman J 2010) Scopes too flexible...and too stiff *IEEE Pulse* **1(3)** 26 –41

[24]Swain P, Ewers R, Peh R, Sadaat V 2005 New measurement methods and a randomized comparison of force transmission using flexible endoscopes and instruments before and after the application of ShapeLock TM technology. *Gastrointest. Endosc.* **61** 241

[25]Eickhoff A, Jakobs R, Kamal A, Mermash S, Riemann J F, Van Dam J 2006 In vitro evaluation of forces exerted by a new computer-assisted colonoscope (the NeoGuide Endoscopy System) *Endoscopy* **38(12)**1224-9

[26]Kim Y J, Cheng S, Kim S and Iagnemma K 2013 A Novel Layer Jamming Mechanism With Tunable Stiffness Capability for Minimally Invasive Surgery *IEEE Trans. Rob.* **29(4)**1031-42

[27] Kim Y J, Cheng S, Kim S and Iagnemma K 2013 A Stiffness-Adjustable Hyperredundant Manipulator Using a Variable Neutral-Line Mechanism for Minimally Invasive Surgery. *IEEE Trans. Rob.***30** 1-14

[28] Moses M S, Kutzer M D M and Ma H, Mehran A 2013 A continuum manipulator made of interlocking fibers *Proc. IEEE Int. Conf. on Robotics and Automation* pp 4008-015

[29] Cianchetti M, Ranzani T, Gerboni G, De Falco I, Laschi C, Menciassi A 2013 STIFF-FLOP Surgical Manipulator: mechanical design and experimental characterization of the single module. *Proc. IEEE/RSJ Int. Conf. on Intelligent Robots and Systems* pp 3576-581

[30] Dhumane P W, Diana M, Leroy J and Marescaux J 2011 Minimally invasive single-site surgery for the digestive system: A technological review. *J. Min. Access Surg.* **7(1)** 40

[31] Jennie YY and Yu Ho W K 2013 Hurdles and highlights in the development of a novel robotic platform for endoscopic surgery *Gastrointestinal Intervention* **2(2)**87-89

[32] Brown E, Rodenberg N, Amend J, Mozeika A, Steltz E, Zakin MR, et al. Universal robotic gripper based on the jamming of granular material. Proc Natl Acad Sci U S A 2010;107:18809–14

[33] Steltz E, Mozeika A, Rembisz J, Corson N, Jaeger HM. Jamming as an Enabling Technology for Soft Robotics. SPIE 2010;7642:764225.

[34] Jiang A, Xynogalas G, Dasgupta P, Althoefer K, Nanayakkara T. Design of a variable stiffness flexible manipulator with composite granular jamming and membrane coupling. 2012 IEEE/RSJ Int. Conf. Intell. Robot. Syst., IEEE; 2012, p. 2922–7.

[35] M. Li, T. Ranzani, S. Sareh, L. Seneviratne, P. Dasgupta, H. Wurdemann, K. Althoefer. (2014). Multi-Fingered Haptic Palpation utilizing Granular Jamming Stiffness Feedback Actuators. Accepted for publication in Smart Materials and Structures (SMS).

[36] Melzer A., Buess G. and Cuschieri A.1994 Instrumentation and allied technology for endoscopic surgery *Operative Manual of Endoscopic Surgery*, vol. 2, A. Cuschieri, G. Buess, and J. Perissat, Eds. Berlin, Germany: Springer-Verlag, 1994.

[37] N.Y. Mehta, R.S. Haluck, M.I. Frecker, A.J. Snyder. (2001). Sequence and task analysis of instrument use in common laparoscopic procedures. Surgical Endoscopy And Other Interventional Techniques. Volume 16, Issue 2, pp 280-285